



Bachelor Project
Modeling of a PEM Electrolyzer

Supervisors

Prof. Mario PAOLONE
Rahul GUPTA

Author: Cem KESKE

June 17, 2021

Contents

1	Introduction	3
1.1	Project description	3
1.2	PEM electrolyzer	3
1.3	Project objectives	3
2	Models	4
2.1	Power Reference Tracking Model	4
2.1.1	Estimating the time constant with τ -threshold	5
2.1.2	Estimating the time constant with OLS fitting	7
2.1.3	Negative-step behavior	8
2.2	Electrical stack model & Equivalent Circuit	9
2.2.1	Model and simplification procedure	9
2.2.2	Reversible voltage	11
2.2.3	Diffusion Overvoltage	12
2.2.4	Activation Overvoltage	13
2.2.5	Ohmic Overpotential	13
2.2.6	Proof of convexity	14
2.2.7	Parameter fitting using experimental data	15
2.2.8	Power Efficiency	17
2.3	Hydrogen production and tank models	18
2.3.1	Experiments and Faradaic efficiency	19
2.3.2	Tank filling simulations	20
2.4	Thermal Model	21
2.4.1	Thermal circuit	22
2.4.2	Estimation of passive components	23
2.4.3	Cooling system model	25
2.4.4	Temperature assumption and model simplification	26
3	Conclusion	26
Appendix: MATLAB Files		28

1 Introduction

1.1 Project description

While the efficiency of the hydrogen energy production and storage systems are increasing, the possibility of using these systems in micro-grids for storage and heating is in research, as in [1]. The DESL lab at EPFL has an experimental micro-grid including a hydrogen energy storage system, which gets replaced in 2021 because the old electrolyzer stack and the fuel cell was at the end of their lives. The electrolysis system is used to provide hydrogen pressurized at 30 bar for use by the fuel cell, acting as a power consumer on the DESL micro-grid. 400V AC power is provided by the micro-grid to the electrolyzer. The control system of the electrolyzer is powered by the normal power grid. The electrolyzer can be controlled via CAN by DESL software agents.

1.2 PEM electrolyzer

An electrolyzer is a system which is capable of breaking water into hydrogen (H_2) and oxygen (O_2) molecules using electrical current. In PEM (proton-exchange membrane or polymer-electrolyte membrane) electrolyzers, this is done by a membrane placed between the cathode and anode, enabling the protons to diffuse from the anode to the cathode by passing inside the membrane, leaving (O_2) to form in the anode and form (H_2) at the cathode by combining with electrons supplied by the current (or voltage) source, as seen in figure 1.

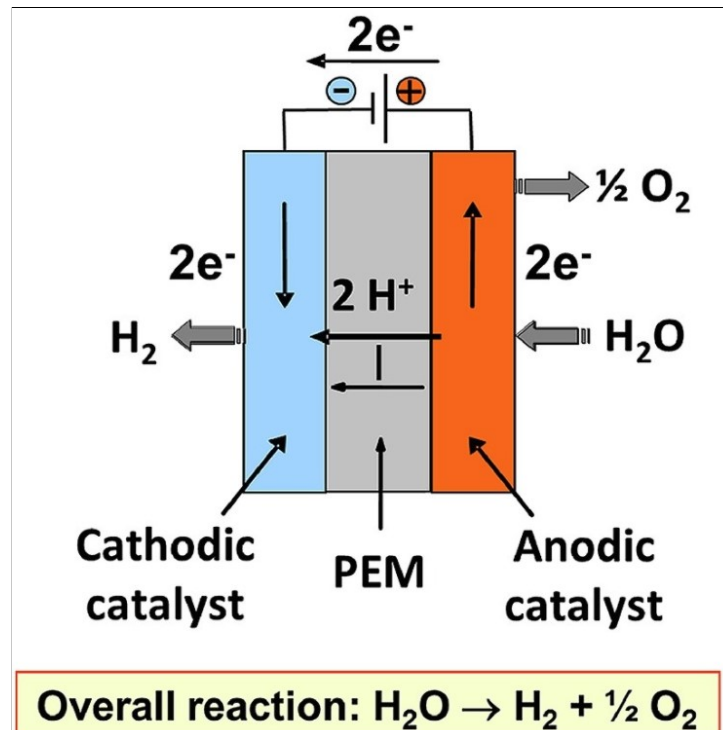


Figure 1: PEM Electrolyzer Cell Model [2]

1.3 Project objectives

The aim of this project is to establish a model for the electrolyzer so that it can be integrated in the model predictive control algorithm in [3]. From the grid's point of view, we are able

to control the reference power that we want the electrolyzer to consume, and we want to be able to predict the outcome (efficiency, produced hydrogen) via the established model. We will cover the subjects one by one and establish a model similar to the one in figure 2. The different elements are:

- **Power tracking model:** Explaining the evolution of the instantaneous power used by the stack according to the reference power set by the control algorithm. This is useful to determine how fast the electrolyzer power can be changed as the electrolyzer is seen as a variable load in the grid.
- **Electrical stack model:** This model explains the behavior of the stack as an electrical circuit at given temperatures. We will first establish the model $V(T, I)$. Then for a given stack temperature and current, we can find the voltage, likewise, for a given power and temperature, we can find the voltage and the current. Knowing $P = V \cdot I$, there are multiple couples of V and I which could give the same power. However, with the electrical model, at a fixed temperature, we are aiming to find a unique couple of V and I .
- **Hydrogen production model:** This model will allow us to compute the generated hydrogen in terms of the stack current. Using the generated hydrogen, we can define the output power of the stack and have an idea on the efficiency.
- **Tank model:** The produced hydrogen flows to the tank and increases the tank pressure to a maximum level of 30 bar. The hydrogen level in the tank is given in terms of the tank pressure, for example 15 bars of pressure means the tank is 50% full.
- **Thermal model:** The process of hydrogen generation can never reach 100% efficiency. Hence, there's always some heat generated during the electrolysis reaction. For this reason, a cooling system controls the temperature of the stack, where the cooling temperature can be set as an input parameter. This model will allow us to determine the stack temperature taking into account both the heat generated by the losses and taken away by the cooling system. We will also try to analyze if the stack temperature can be kept constant, which would notably simplify the model.

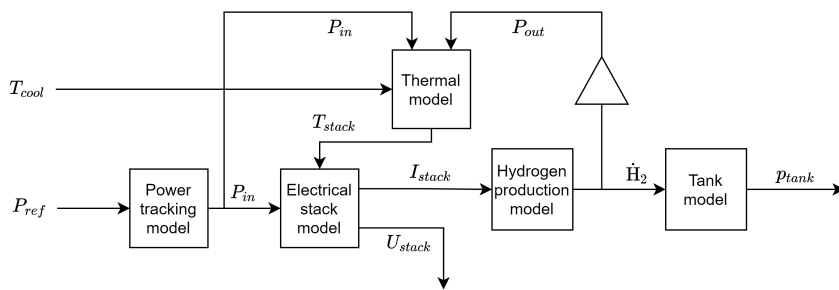


Figure 2: Aimed model to establish

2 Models

2.1 Power Reference Tracking Model

From the grid's perspective, we are only able to control the power used by the electrolyzer. However, this power can't be changed instantly. For this reason, we need to model the system

in figure 3, connecting the reference power to the real-time input power. Therefore, it's needed to perform experiments with a step change in the reference power level and observe the behavior of the real-time input power, to know how fast the input power can be changed. The result of the step response tests can be seen in figures 4 and 5.

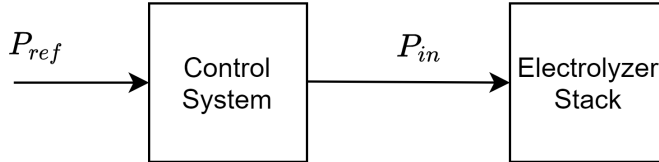


Figure 3: Power reference tracking model

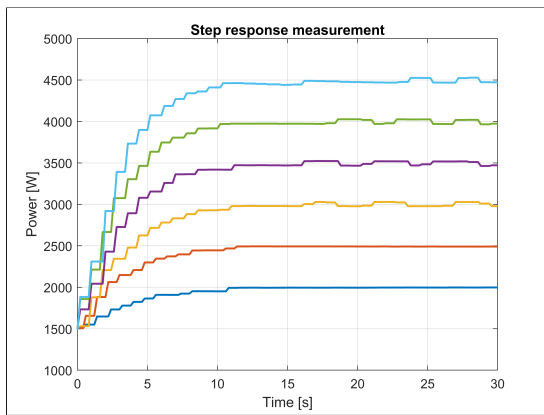


Figure 4: Power step response

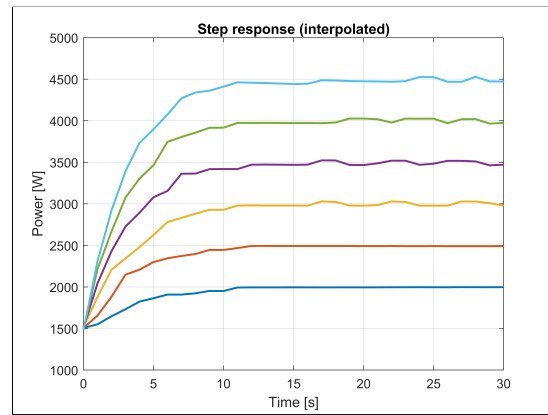


Figure 5: Power step response (interpolated)

Looking at the step responses in figures 4 and 5, we decided to model the reference-to-input power behavior using a first order system, as given in Laplace domain:

$$\frac{P_{in}}{P_{ref}} = \frac{1}{1 + \tau_p s} \quad (1)$$

Thus, for a step of the reference power from P_0 to P_1 at $t = 0$, with $P_{step} = P_1 - P_0$, we have:

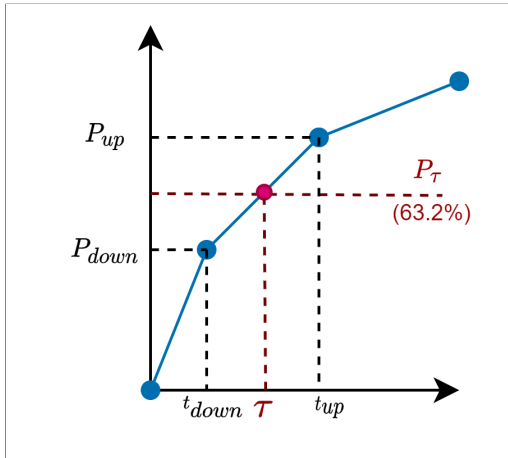
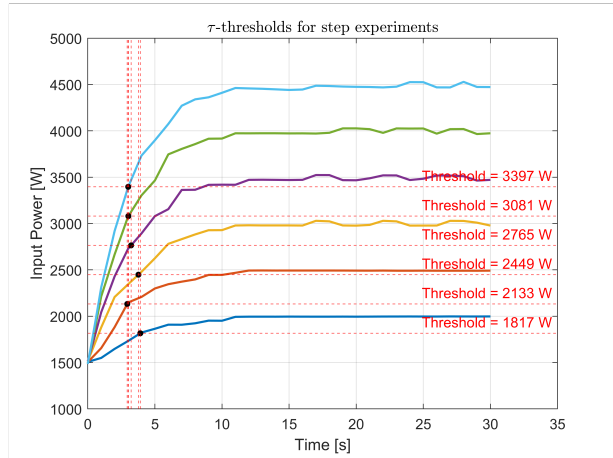
$$P_{in}(t) = P_0 + P_{step} \left(1 - e^{-\frac{t}{\tau_p}} \right) \quad \text{for } t > 0 \quad (2)$$

To be able to use this model for control purposes, we have to estimate the parameter τ_p using the experiments. Two different ways to estimate this parameter are given in the subsections below.

2.1.1 Estimating the time constant with τ -threshold

By equation 2, we know that the time instant that the input power reaches 63.2% of its step is given by τ_p . As the sample rate isn't fast enough to determine a precise τ_p , we used linear interpolation to estimate τ_p at each step response experiment. The 63.2% thresholds and their corresponding power values are shown in figure 7. Referring figure 6, from the interpolated graph, using two sample points around 63.2% threshold τ_p can be found as:

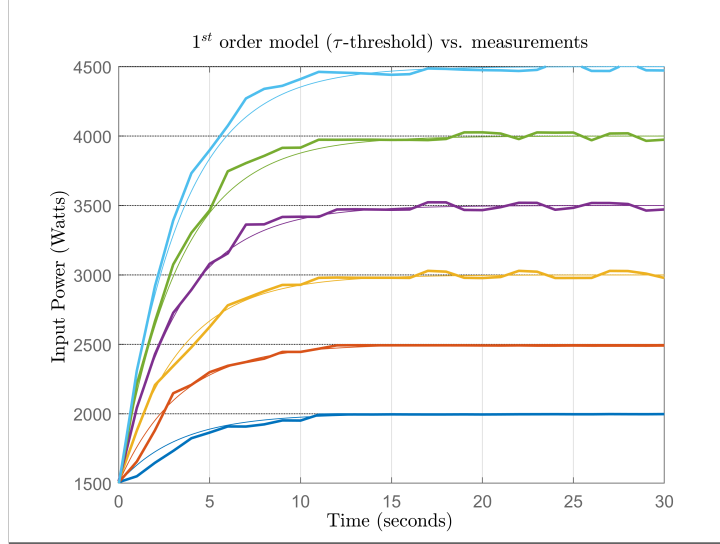
$$\tau_p = \frac{t_{up}(P_\tau - P_{down}) + t_{down}(P_{up} - P_\tau)}{P_{up} - P_{down}} \quad (3)$$

Figure 6: Estimating τ from interpolationFigure 7: τ -threshold method

For each measurement, it's possible to determine a τ as shown in figure 7. Due to the poor sample rate and interpolation, the time constant is not the same for each measurement, however they are very close. To describe the behavior of the system, in an experiment with N measurements, we defined our time constant estimator as the average of measurements:

$$\hat{\tau} = \frac{1}{N} \sum_{i=1}^N \tau_i \quad (4)$$

τ_p is found to be 3.31 s using this approach. The system is simulated using this time constant and compared with the actual measurements as shown in figure 8.

Figure 8: First order model with τ -threshold vs. measurements

2.1.2 Estimating the time constant with OLS fitting

From equation 2 we can deduce the time derivative of the input power step response. Then we can use it to get the following identity:

$$\frac{dP_{in}(t)}{dt} = \frac{P_{step}}{\tau_p} \cdot e^{-\frac{t}{\tau_p}} \quad \Rightarrow \quad P_{step} \cdot e^{-\frac{t}{\tau_p}} = \tau_p \cdot \frac{dP_{in}(t)}{dt} \quad \text{for } t > 0 \quad (5)$$

By substituting the result of equation 5 in equation 2 we get:

$$P_{in}(t) = P_0 + P_{step} - \tau_p \cdot \frac{dP_{in}(t)}{dt} \quad \text{for } t > 0$$

As we have a discrete time step and not a continuous signal, we discretize the equation using first order backwards derivative approximation:

$$p_i = P_0 + P_{step} - \frac{\tau_p}{T_s} \cdot (p_i - p_{i-1}) \quad (6)$$

where p_i is the input power measurement at time t_i , and T_s is the sampling period. We will search to minimize least-squares errors:

$$\hat{\tau}_p = \arg \min_{\tau_p} \sum_{i=1}^N \left\| p_i - P_0 - P_{step} + \frac{\tau_p}{T_s} \cdot (p_i - p_{i-1}) \right\|^2$$

Equation 6 can be extended to all N samples of the step input using matrix notation and introducing \mathbf{X} and \mathbf{Y} matrices:

$$T_s \cdot \begin{bmatrix} p_1 - P_0 - P_{step} \\ \vdots \\ p_N - P_0 - P_{step} \end{bmatrix} = -\tau_p \cdot \begin{bmatrix} p_1 - p_0 \\ \vdots \\ p_N - p_{N-1} \end{bmatrix} \quad \Rightarrow \quad -T_s \cdot \mathbf{Y} = \mathbf{X} \cdot \tau_p$$

\mathbf{X} and \mathbf{Y} matrices are obtained directly from the measurements. Then the OLS solution is simply given as:

$$\hat{\tau}_p = -T_s \cdot (\mathbf{X}^T \mathbf{X})^{-1} \mathbf{X}^T \mathbf{Y} \quad (7)$$

τ_p is found to be 3.04 s using this approach. The system is simulated using this time constant and compared with the actual measurements as shown in figure 9.

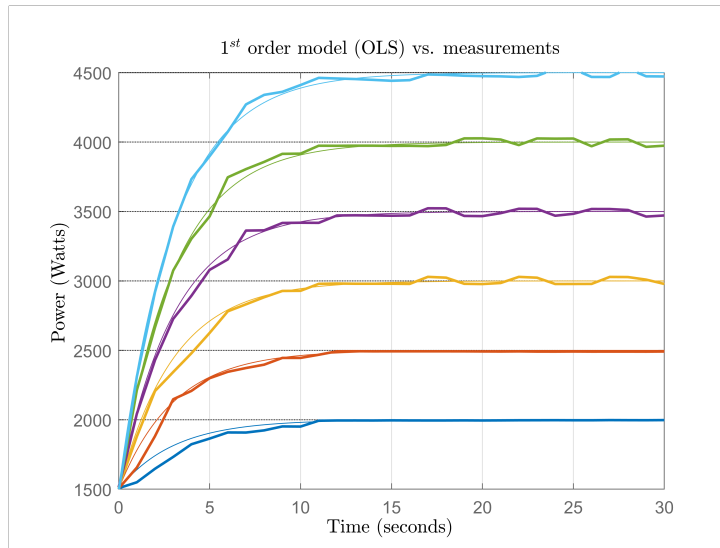


Figure 9: First order model with OLS vs. measurements

2.1.3 Negative-step behavior

For a positive step of the input power, we've seen that a first-order model can be used and the time constant shows good reproducibility at each step response. For a negative step, the τ_p determined in the sections above is reproducible when the step is less than or equal to 2 kW. However, during a negative step, if the step is larger than 2 kW, there's a nearly-instant drop first, then some random-looking time of stable operation, followed again by a first-order negative step response. To be able to describe this effect, we would need more experiments to understand the process creating the random-looking waiting time. However, because of technical reasons, new experiments couldn't be realized by the time of writing this report. The procedure should be straightforwardly the same if the waiting time is well-defined.

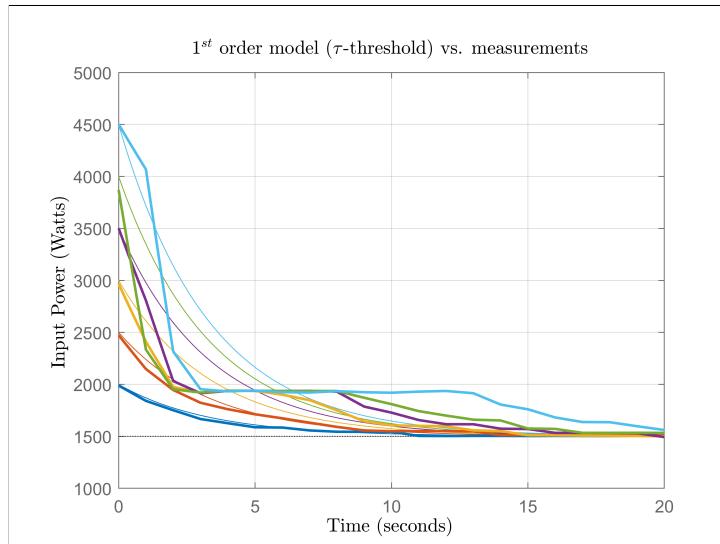


Figure 10: Negative power step

2.2 Electrical stack model & Equivalent Circuit

2.2.1 Model and simplification procedure

The presented cell from figure 1 is often connected in series with many identical cells to form electrolyzer stacks as shown in figure 11, implying for the stack current I_{stack} and the stack voltage V_{stack} in a stack with N cells :

$$I_{stack} = I_n \quad \forall n \quad \text{and} \quad V_{stack} = \sum_{n=1}^N V_n \quad (8)$$

Where I_n and V_n denotes the current and the voltage of the n'th cell respectively. We will be modeling a pressurized stack, meaning that the hydrogen outlet of the cathode is naturally pressurized. This enables a hydrogen production process avoiding additional need for compression [4].



Figure 11: The electrolyzer stack at EPFL, DESL

For control purposes, we are searching a model to describe the voltage of a cell using the instantaneous stack current I and the stack temperature T , and we will need to use a set (vector) containing p parameters: $\vec{\beta} \in \mathbb{R}^p$:

$$V_{cell} = f_{\vec{\beta}}(I, T) \quad \Rightarrow \quad V_{stack} = n_{cells} \cdot f_{\vec{\beta}}(I, T)$$

The idea here is to be able to reduce the degrees of freedom of the system, i.e. the voltage can be found if the current and the temperature is known, or the current can be found if the temperature and voltage is known. These conditions imply that when one of the variables is fixed, the mapping between the other two should be one-to-one. For example if the temperature is fixed to T_0 , for each positive value of current I we should be getting a different V , otherwise, this is against the determinism of the model, and means that we left unexplained non-constant processes in the model causing the voltage to change independently from the current and the temperature.

After establishing a function f , we will perform a fitting, minimizing the sum of squared-errors between the experimental voltages and the voltages predicted by the model. Let $S_i = \{V_i, I_i, T_i\}$ be the i 'th sample from the experiment where the voltage, current and the temperature of the stack is observed. To estimate the parameters $\vec{\beta}$ of the system, we will use the cost function:

$$L(\vec{\beta}) = \sum_{i=1}^N \left\| n_{cells} \cdot f_{\vec{\beta}}(I_i, T_i) - V_i \right\|^2 \quad (9)$$

Then, we will try to find the set of parameters which would minimize this cost. Hence, the estimated parameters of the system will be given by the solution of the problem:

$$\hat{\vec{\beta}} = \arg \min_{\vec{\beta}} L(\vec{\beta})$$

Different algorithms could be used to solve this problem, all depending on the cost function. If the cost function is convex in terms of the parameter vector $\vec{\beta}$, then the problem admits a global solution which could be found easily using gradient descent or even given implicitly. However, if the cost function is not convex, greedy gradient descent algorithms could converge to local minimums of the cost function, and we can find a non-optimal parameter set. Thus, we would have to choose the parameter ranges and starting points carefully.

For this reason, we will search to simplify the function f as much as possible, and manipulate it such that it guarantees to have a convex cost function, all making sure that we're not giving up performance for simplicity, because it wouldn't make sense to have a very simple model if it doesn't explain the behavior of the system on our operating points. Therefore, in the following subsections, we tried to empirically minimize the number of unknown parameters, and searched to simplify the expressions in accordance with the literature to get a convex cost function $L(\vec{\beta})$.

The convexity of $L(\vec{\beta})$ on the parameter space can be checked by calculating its Hessian matrix respect to the parameter vector and showing that it is positive semi-definite, in other words, all eigenvalues of the Hessian matrix should be non-negative to guarantee convexity.

$$\mathbf{H}_{\vec{\beta}}(L) = \begin{bmatrix} \frac{\partial^2 L}{\partial \beta_1^2} & \frac{\partial^2 L}{\partial \beta_1 \partial \beta_2} & \cdots & \frac{\partial^2 L}{\partial \beta_1 \partial \beta_p} \\ \frac{\partial^2 L}{\partial \beta_2 \partial \beta_1} & \frac{\partial^2 L}{\partial \beta_2^2} & \cdots & \frac{\partial^2 L}{\partial \beta_2 \partial \beta_p} \\ \vdots & \vdots & \ddots & \vdots \\ \frac{\partial^2 L}{\partial \beta_p \partial \beta_1} & \frac{\partial^2 L}{\partial \beta_p \partial \beta_2} & \cdots & \frac{\partial^2 L}{\partial \beta_p^2} \end{bmatrix} \quad (10)$$

To start, the electrical model from [5] will be used for the electrolyzer cells (in a much simpler version), shown in figure 12 of this report. From [2], it is seen that this model is widely used for modeling electrolyzer cells. The elements of the model can be summarized as:

- U_{rev} , the reversible reaction voltage
- u_{diff} , the diffusion overpotential
- u_{act} , the activation overpotential
- u_{ohm} , ohmic overpotential

Each of these components are analyzed in the following sections.

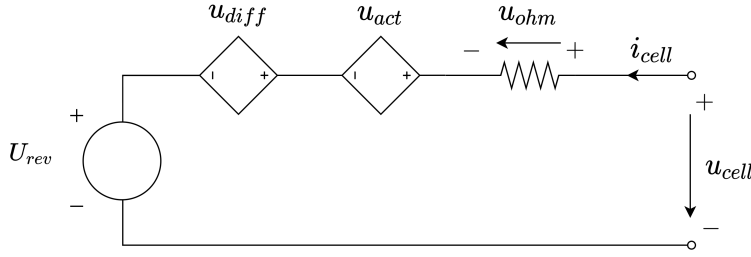


Figure 12: The circuit model of the electrolyzer

2.2.2 Reversible voltage

The reversible voltage is the voltage measured when a negligible amount of current is passing through the cells, representing the standard electrode potential at a given temperature and concentration of the reactive components. This is the theoretical minimum possible cell voltage for electrolysis reaction. From the Nernst equation in [6] and [7], this potential is calculated as:

$$U_{rev} = U^0 + \frac{RT}{nF} \cdot \ln \left(\frac{p_{\text{H}_2} \sqrt{p_{\text{O}_2}}}{p_{\text{H}_2\text{O}}} \right) \quad (11)$$

Where p is the pressure of the reactants and products. These pressures are kept constant at their nominal values by a control system to be able to work in steady state operation. In the electrolyzer datasheet, it is suggested to use the pressure levels equal to their nominal values. However, as we have a specialized control system, in figures 13, 14 and 15, we plotted the histograms of the sensor readings during the experiments to verify that they can be considered constant.

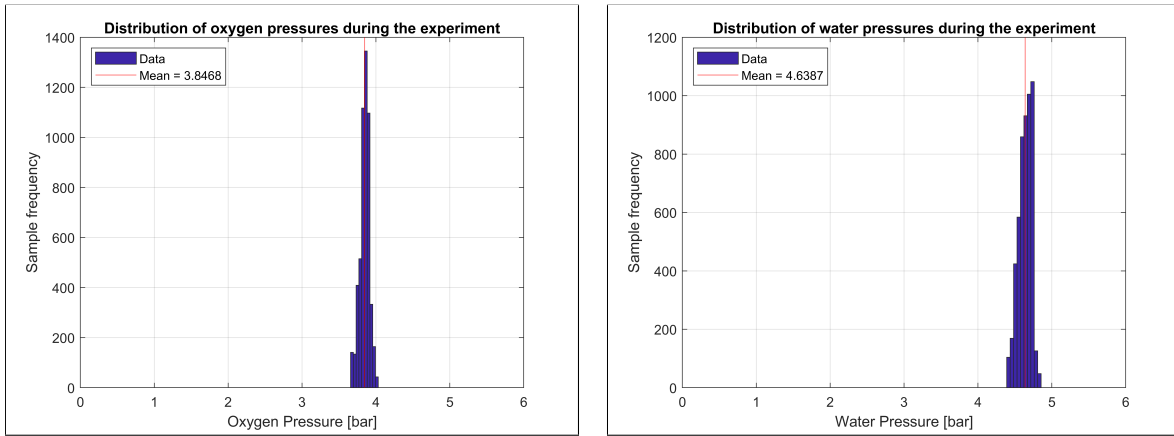


Figure 13: Reaction cell oxygen pressures

Figure 14: Reaction cell water pressures

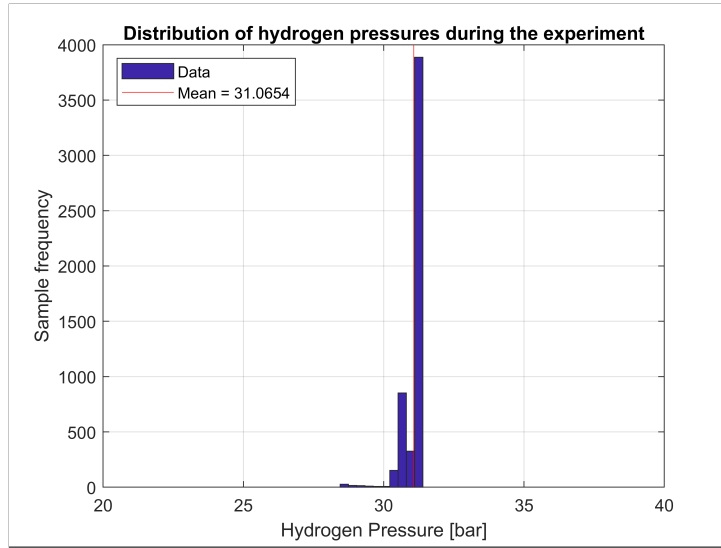


Figure 15: Reaction cell hydrogen pressures

We see that the deviation of the pressures are too small, then using the mean values, we get the reversible reaction voltage:

$$U_{rev} = 1.4813 + 1.11 \cdot 10^{-4} \cdot T_{stack}$$

2.2.3 Diffusion Overvoltage

The diffusion overpotential is caused by the mass transport limitations through the membrane [5]. It's given by this formula in [5] and [8]:

$$u_{diff} = \frac{RT_{an}}{4F} \cdot \ln \left(\frac{C_{O_2}}{C_{O_2ref}} \right) + \frac{RT_{cat}}{2F} \cdot \ln \left(\frac{C_{H_2}}{C_{H_2ref}} \right)$$

where R is the ideal gas constant, T_{an} and T_{cat} are the temperatures of the anode and the cathode, F is the Faraday constant, C_{H_2} and C_{O_2} are the reactant concentrations at the anode and the cathode, C_{H_2ref} and C_{O_2ref} are parameters to estimate for the system.

When the current density through the cell is too high, the concentration of the ions on the surface of the membrane creates a resistance opposing the flow [5]. This increases the ion concentrations on the surface of the membrane. However, the dependence of this membrane surface concentrations to the stack current is hardly observed in commercial electrolyzers as the current densities through the stack are relatively low [4]. Furthermore, the nominal currents in commercial electrolyzers are designed to be low enough, so that it won't saturate the membrane concentrations. In [8] it's demonstrated that the concentrations don't vary much with the current in the stack and can be considered as constant. Thus, the hydrogen and oxygen concentrations are assumed independent of the current. Moreover, we assumed and verified experimentally that:

$$T_{an} \approx T_{cat} \approx T_{stack} \quad (12)$$

Hence, the diffusion overvoltage simplifies to:

$$u_{diff} = T \cdot \left\{ \frac{R}{2F} \left[\frac{1}{2} \ln \left(\frac{C_{O_2}}{C_{O_2ref}} \right) - \ln \left(\frac{C_{H_2}}{C_{H_2ref}} \right) \right] \right\}$$

We made the assumption that the right side of this equation is constant as stated before, therefore we use the diffusion overpotential as:

$$u_{diff} \approx a \cdot T \quad (13)$$

where a is an empirical parameter to estimate by model fitting.

2.2.4 Activation Overvoltage

The activation overpotential reflects the energy losses to overcome the activation energy of the cell reaction, caused by the accumulation of electrons at the electrode surface, producing an energy barrier for the incoming electrons [9]. This phenomenon can be modelled by Tafel's expression, as suggested by [4], for anode and cathode respectively:

$$u_{act,an} = \frac{R T}{F} \cdot \ln \left(\frac{i}{2 i_{0,an}} \right) = \frac{R T}{F} \cdot \ln \left(\frac{I_{stack}}{2 i_{0,an} A_m} \right) \quad (14)$$

$$u_{act,cat} = \frac{R T}{F} \cdot \ln \left(\frac{i}{2 i_{0,cat}} \right) = \frac{R T}{F} \cdot \ln \left(\frac{I_{stack}}{2 i_{0,cat} A_m} \right) \quad (15)$$

A large range of values for $i_{0,an}$ (from 10^{-6} to 10^{-13}) and $i_{0,cat}$ (from 10^{-3} to 10^{-12}) are proposed in the literature [5]. The values for i_{an} and i_{cat} are estimated empirically in [4] and there's no straightforward calculation to perform to find this reference current. For this reason, this is left as a model parameter to estimate. However, these functions caused the overall fitting cost function mentioned in subsection 2.2.1 to be non-convex. So, an empirical simplification should be made in order to describe this behavior. For the activation overvoltage in a PEM cell, [1] considers the two overvoltages at anode and cathode described by Tafel's equation together, furthermore, replaces the logarithm function with a square root as they have a similar shape, and introduces a linear temperature dependence term. By doing so, we get empirically:

$$u_{act} = (b + c \cdot T) \cdot \sqrt{I_{stack}} \quad (16)$$

where b and c are empirical parameters to estimate by model fitting.

2.2.5 Ohmic Overpotential

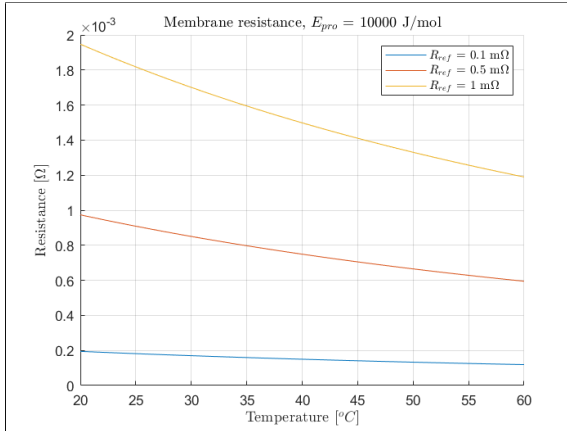
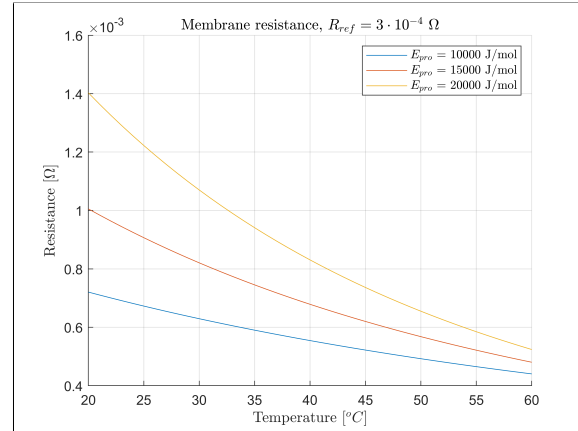
The stack water purity and conductivity is continuously monitored by sensors. The conductivity of the water is always kept as small as possible using filters to eliminate the chemicals and ionized minerals from the water. This is needed to force all the current to circulate via the membrane by exchanging protons, instead of using the ionized current carriers (electrons and ions) inside the water. Hence, the conductivity of a cell is modeled only by the membrane conductivity, by neglecting the electrode and conductor resistances. For the evolution of the conductivity (in [S/m]) of a PEM membrane, [4] suggests:

$$\sigma(T) = \sigma_{ref} \exp \left[\frac{-E_{pro}}{R} \left(\frac{1}{T} - \frac{1}{T_{ref}} \right) \right] \quad (17)$$

where T_{ref} and σ_{ref} are reference quantities to choose and E_{pro} is the proton-exchange activation energy to estimate. Then the total resistance of a single cell would be given by the resistivity law:

$$R_{cell}(T) = \rho(T) \frac{\delta_m}{A} = \frac{\delta_m}{A \sigma(T)} = R_{ref} \cdot \exp \left[\frac{E_{pro}}{R} \left(\frac{1}{T} - \frac{1}{T_{ref}} \right) \right] \quad (18)$$

where δ_m and A is the membrane thickness and membrane area values. [8] follows a literature search, and suggests from 10^5 J/mol to $2 \cdot 10^5 \text{ J/mol}$ for E_{pro} , and chooses R_{ref} as $3.7 \cdot 10^{-4} \Omega$. Since T_{ref} and R_{ref} gives the same degree of freedom when the exponential function is expanded, we fix T_{ref} around our working point and choose 350K. After performing the Hessian matrix analysis in subsection 2.2.1, it's seen that the exponential function contributed to the non-convexity of the overall cost, so a simplification should be performed in line with the literature. We see from figures 16 and 17 that the temperature dependence can be brutally simplified to a

Figure 16: PEM resistance for R_{ref} valuesFigure 17: PEM resistance for E_{pro} values

linear function, and the two parameters adjust the height and the slope of that linear function. For this reason, we choose to approximate the membrane resistance by a linear function with two parameters. In [1], we see that the same approximation is made to describe the PEM resistance dependence on temperature, so we use the same linear function:

$$R_{cell}(T) = d + T \cdot h \quad (19)$$

where d and h are empirical parameters to estimate by model fitting, with the constraint that d is negative and h is positive. Then the ohmic overpotential is given by:

$$u_{ohm} = R_{cell}(T) \cdot I_{stack} \quad (20)$$

2.2.6 Proof of convexity

Combining equations 11, 13, 16 and 20 we get the final expression of the cell voltage for the model presented in subsection 2.2.1:

$$f_{\vec{\beta}}(I, T) = 1.4813 + 1.11 \cdot 10^{-4} \cdot T + a \cdot T + (b + c \cdot T) \cdot \sqrt{I} + (d + h \cdot T) \cdot I \quad \text{with} \quad \vec{\beta} = \begin{bmatrix} a \\ b \\ c \\ d \\ h \end{bmatrix} \quad (21)$$

To prove the convexity of the cost function, at each simplification of the model, we computed the hessian matrix of the cost and tested if it's positive semi-definite. For the final model that we have in equation 21, we give the proof below that it's convex (in fact this can also be seen directly as the function is linear in terms of the parameters). Separating the cost function (eq. 9) to costs per sample, we get:

$$L_i(\vec{\beta}) = \left\| n_{cells} \cdot f_{\vec{\beta}}(I_i, T_i) - V_i \right\|^2 \quad \Rightarrow \quad L(\vec{\beta}) = \sum_{i=1}^N L_i(\vec{\beta})$$

Then using the linearity of the derivatives, we get:

$$\mathbf{H}_{\vec{\beta}}(L) = \sum_{i=1}^N \mathbf{H}_{\vec{\beta}}(L_i)$$

From the definition of positive semi-definiteness, it's trivial that the sum of two positive semi-definite matrices is also positive semi-definite. So we know that $\mathbf{H}_{\vec{\beta}}(L)$ is positive semi-definite if each $\mathbf{H}_{\vec{\beta}}(L_i)$ is positive semi-definite. By computing $\mathbf{H}_{\vec{\beta}}(L_i)$ we see that its only non-zero eigenvalue is: $\lambda_i = 2I_i^2T_i^2 + 2I_i^2 + 2I_iT_i^2 + 2I_i + 2T_i^2$. The non-negativity of this eigenvalue is guaranteed if we have $I_i > 0$ and $T_i > 0$ for each sample, which is the case. So the convexity of the cost function is guaranteed. Furthermore, it can be seen that the model is a linear model (respect to the parameters), and an OLS linear regression could be used to solve this problem. To be more precise, by introducing an error term ε_i for each sample $S_i = \{V_i, I_i, T_i\}$, we should be able to write the measurements as:

$$V_i = 1.4813 + 1.11 \cdot 10^{-4} \cdot T_i + a \cdot T_i + (b + c \cdot T_i) \cdot \sqrt{I_i} + (d + h \cdot T_i) \cdot I_i + \varepsilon_i \quad (22)$$

As stated before, with the hypothesis that these errors are normally distributed, we will try to minimize the sum of squared errors $(\sum_{i=1}^N \varepsilon_i^2)$ by adjusting the parameters $\vec{\beta}$. The equation above can be extended to each sample using matrix notation:

$$\begin{bmatrix} V_1 - 1.4813 - 1.11 \cdot 10^{-4} \cdot T_1 \\ V_2 - 1.4813 - 1.11 \cdot 10^{-4} \cdot T_2 \\ \vdots \\ V_N - 1.4813 - 1.11 \cdot 10^{-4} \cdot T_N \end{bmatrix} = \begin{bmatrix} T_1 & \sqrt{T_1} & T_1\sqrt{T_1} & I_1 & T_1I_1 \\ T_2 & \sqrt{T_2} & T_2\sqrt{T_2} & I_2 & T_2I_2 \\ \vdots & & \vdots & & \\ T_N & \sqrt{T_N} & T_N\sqrt{T_N} & I_N & T_NI_N \end{bmatrix} \cdot \begin{bmatrix} a \\ b \\ c \\ d \\ h \end{bmatrix} + \begin{bmatrix} \varepsilon_1 \\ \varepsilon_2 \\ \vdots \\ \varepsilon_N \end{bmatrix} \quad (23)$$

As we previously did in section 2.1.2, we can again introduce \mathbf{X} and \mathbf{Y} matrices representing the measurements that we made:

$$\mathbf{Y} = \mathbf{X} \cdot \vec{\beta} + \begin{bmatrix} \varepsilon_1 \\ \varepsilon_2 \\ \vdots \\ \varepsilon_N \end{bmatrix} \quad (24)$$

\mathbf{X} and \mathbf{Y} matrices are obtained directly from the measurements. Then the OLS solution is simply given as:

$$\hat{\vec{\beta}} = (\mathbf{X}^T \mathbf{X})^{-1} \mathbf{X}^T \mathbf{Y} \quad (25)$$

2.2.7 Parameter fitting using experimental data

To generate the data needed for the fitting, tests on the stack were done. At controlled temperatures of 30, 40 and 50°C, we swept a range of power inputs [1500 W – 4500 W] with steps of 500W. At least 10 minutes of operation is observed at each power input. The experiment process and the collected samples are given in figures 18 and 19.

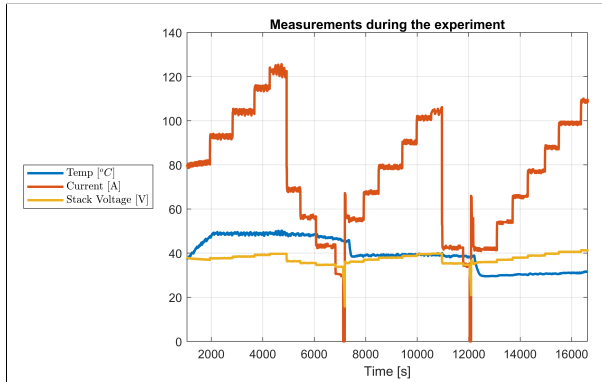


Figure 18: Experiment timeline

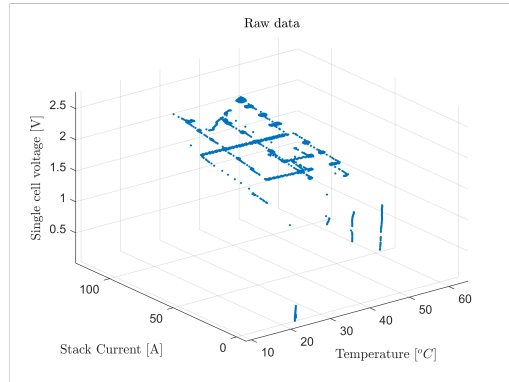


Figure 19: Raw data

The raw data that we got from the electrolyzer also contains unnecessary measurements, for example, some points where an error is generated, production is paused, measurements without current, or simply erroneous and distorted measurements because of fast transitions. For this reason, we needed to clean the data up first. During the experiment, we ran the electrolyzer for at least 10 minutes at each power input. With 1 Hz sample rate, the points where measurements were taken should contain at least 600 samples. So we only used the data around those points and took their centers for fitting.

To be more precise, let \mathcal{I} and \mathcal{T} be the intervals containing all current and temperature values from the experiment. We define the sub-intervals of length 1, \mathcal{I}_i and \mathcal{T}_j spanning the intervals:

$$\mathcal{I} = \bigcup_i \mathcal{I}_i \quad \text{and} \quad \mathcal{T} = \bigcup_j \mathcal{T}_j$$

Then for each set $\mathcal{M}_{ij} = \mathcal{I}_i \times \mathcal{T}_j$, if the corresponding set contains more than 100 samples, we create a new sample containing the average values of the V , I and T , and move each sample in \mathcal{M}_{ij} to that computed centroid. The results are shown in figure 20.

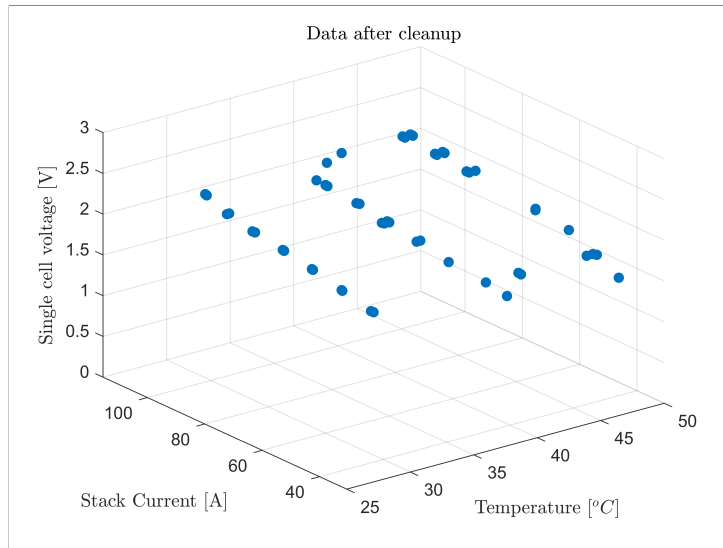


Figure 20: Data after preprocessing

With the preprocessed data from figure 20, we use equation 25 to find the parameters as given in table 1.

Parameter	Estimate	Confidence Interval [95%]
a	$2.35 \cdot 10^{-4}$	[$2.28 \cdot 10^{-4}, 2.42 \cdot 10^{-4}$]
b	$1.67 \cdot 10^{-1}$	[$1.65 \cdot 10^{-1}, 1.69 \cdot 10^{-1}$]
c	$-5.21 \cdot 10^{-4}$	[$-5.28 \cdot 10^{-4}, -5.14 \cdot 10^{-4}$]
d	$9.92 \cdot 10^{-3}$	[$9.97 \cdot 10^{-3}, 10.14 \cdot 10^{-3}$]
h	$-2.08 \cdot 10^{-5}$	[$-2.15 \cdot 10^{-5}, -2.01 \cdot 10^{-5}$]

Table 1: Estimated parameters

	R^2	ε_{rms}
Fitting samples	0.9988	0.0032
Test samples	0.9982	0.0039

Table 2: Fitting performance

We calculated the performance of the chosen parameters both on the fitting data and the raw data in table 2. The results show a good fit and represent the voltage variation very well in the working zone of the electrolyzer. Using these parameters, the obtained model becomes:

$$\begin{aligned} V(I, T) = & 1.4813 + 1.11 \cdot 10^{-4} \cdot T + 2.35 \cdot 10^{-4} \cdot T \\ & + (1.67 \cdot 10^{-1} - 5.21 \cdot 10^{-4} \cdot T) \cdot \sqrt{I} \\ & + (9.92 \cdot 10^{-3} - 2.08 \cdot 10^{-5} \cdot T) \cdot I \end{aligned} \quad (26)$$

To be sure that the model represents the actual behavior, the polarization predictions made by the model and electrolyzer data is compared in figure 21. We also have to check if the performance of the model is different on different operating points. In figure 22, we see that the relative error is usually smaller than 1%, and the error of the model on the raw data is equally distributed in different operating points. This means that the model doesn't perform differently on different operating points.

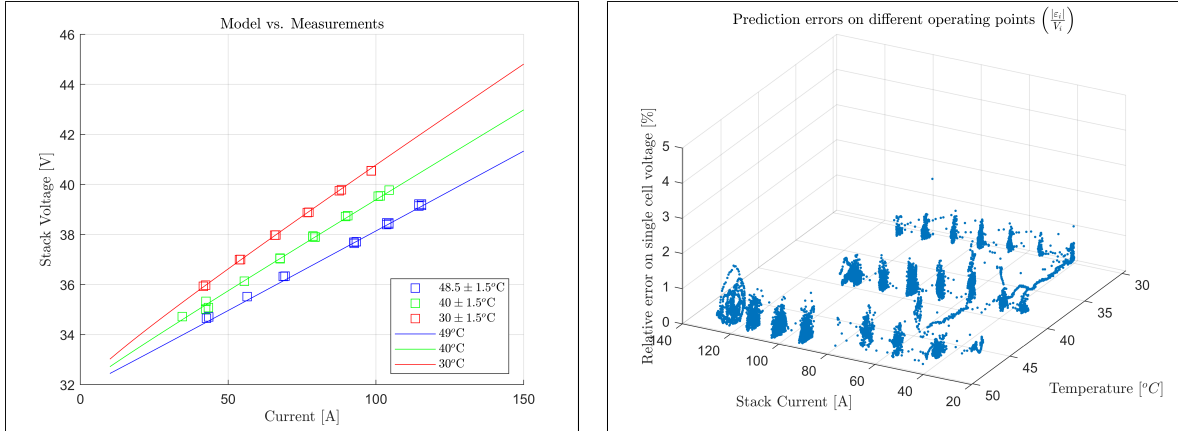


Figure 21: Samples vs. model

Figure 22: Relative error on operating points

2.2.8 Power Efficiency

To calculate the power efficiency we need to describe the used and produced powers. The power consumption and production of the stack is given by:

$$P_{in} = I_{stack} \cdot V_{stack} \quad P_{out} = E_{\text{H}_2} \cdot \dot{V}_{\text{H}_2} \quad (27)$$

where E_{H_2} is the internal energy of hydrogen gas ($285.84 \text{ [kJ/mol]} = 140 \text{ [MJ/kg]}$) and \dot{H}_2 is the hydrogen gas flow rate from the electrolyzer to the tank in $[\text{mol/s}]$. The hydrogen generated by the stack flows to the storage tank thanks to the pressure difference between the stack output and the tank. As the only conduction in the electrolyzer stack is assumed to be due to the displacement of protons through the PEM, the production rate of hydrogen is strictly related to the stack current, as provided in the electrolyzer datasheet, and in [5], [4], [2]. For each electron passing from the circuit, a proton must pass from the proton exchange membrane, thus, \dot{H}_2 flow rate is given by the Faraday equation:

$$\dot{H}_2 = \eta_F \cdot \frac{I}{2F} \cdot n_{cells} \quad (28)$$

where I is the current in $[\text{A}]$, F is the Faraday constant in $[\text{C/mol}]$ and η_F is the Faradaic efficiency of proton exchange membrane. However, this formula can be further simplified if the membrane efficiency is considered as 100%, i.e. there's no current leak due to the conductivity of the water itself. We also see in the electrolyzer datasheet that the Faradaic efficiency is considered as 100%. In section 2.3.1 we also experimentally validate this fact. If there's no Faradaic loss, by using equation 27 we can get the efficiency of the full stack:

$$\eta_{stack} = \frac{P_{out}}{P_{in}} = \frac{E_{H_2} \cdot \dot{H}_2}{n_{cells} \cdot I_{stack} \cdot V_{cell}} = \frac{E_{H_2}}{2 \cdot V_{cell} \cdot F} = \frac{E_{H_2} \cdot n_{cells}}{2 \cdot V_{stack} \cdot F} = n_{cells} \cdot \frac{1.4813 \text{ V}}{V_{stack}} \quad (29)$$

One should note that 1.4813 V is the theoretical minimum cell voltage for the electrolysis reaction to take place. Therefore, this efficiency is always less than unity. According to equation 29 and the model we obtained in equation 26, we can generate the efficiency curves at different operating points as seen in figure 23.

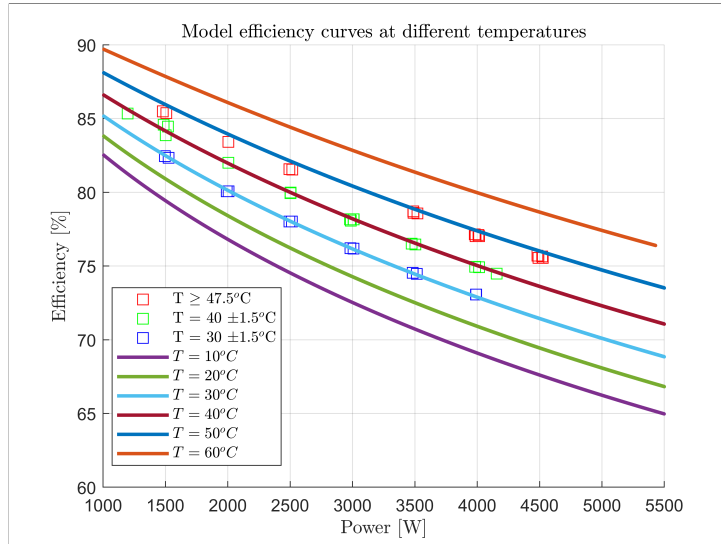


Figure 23: η at fixed temperatures

2.3 Hydrogen production and tank models

The change in the tank pressure can be obtained using the ideal gas law, and the Faraday equation in 28:

$$p_{tank} = \frac{n \cdot R \cdot T_{tank}}{V_{tank}} \quad \Rightarrow \quad \dot{p}_{tank} = \frac{\dot{H}_2 \cdot R \cdot T_{tank}}{V_{tank}} = n_{cells} \cdot \eta_F \cdot \frac{I \cdot R \cdot T_{tank}}{2 \cdot F \cdot V_{tank}} \quad (30)$$

where p_{tank} is the tank pressure in [Pa], R is the ideal gas constant in [J/(K mol)], T_{tank} is the tank temperature in Kelvins, assumed to be constant as there's no measurement, n is the amount of gas in the tank in moles. We have 32 units of 50 liter hydrogen storage tanks, giving a total V_{tank} of 1.6 m³.

We know from equation 30 that the pressure change of the tank at a stable operation point is given by:

$$\Delta p_{tank} = n_{cells} \cdot \eta_F \cdot \frac{\Delta Q_{stack} \cdot R \cdot T_{tank}}{2 \cdot F \cdot V_{tank}}$$

where Δp_{tank} is the tank pressure change during the operation and ΔQ_{stack} is the total charge passed through the stack. Δp_{tank} can be obtained directly from the measurements, and ΔQ_{stack} can be obtained by integrating the current. The tank model is given in the diagram in Laplace domain in figure 24.

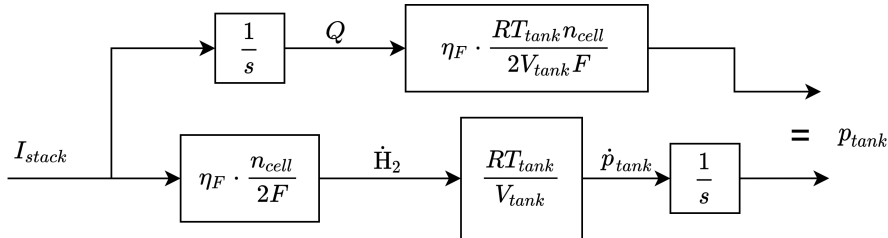


Figure 24: Tank model diagram

2.3.1 Experiments and Faradaic efficiency

To be able to build a complete model and test it experimentally, we use the data in figure 25. As the data from the pressure sensor contains a lot of noise, we will work with the smoothed curve. A moving-mean filter (rectangular window) of 600 samples is used for smoothing, the results were given in figure 25.

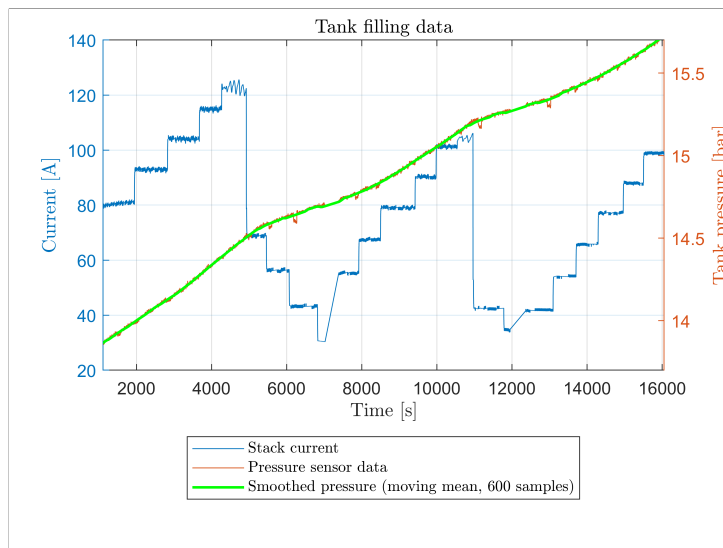


Figure 25: Tank filling data

We use the 19 steady-current operation points that we observed during the experiment in figure

25. By grouping the 19 operation points of the experiment in matrix notation:

$$\begin{bmatrix} \Delta p_{tank,1} \\ \Delta p_{tank,2} \\ \vdots \\ \Delta p_{tank,19} \end{bmatrix} = \eta_F \cdot \begin{bmatrix} k \cdot \Delta Q_{stack,1} \\ k \cdot \Delta Q_{stack,2} \\ \vdots \\ k \cdot \Delta Q_{stack,19} \end{bmatrix} + \begin{bmatrix} \varepsilon_1 \\ \varepsilon_2 \\ \vdots \\ \varepsilon_{19} \end{bmatrix} \quad \text{with } k = n_{cells} \cdot \frac{R \cdot T_{tank}}{2 \cdot F \cdot V_{tank}} \quad (31)$$

Δp_{tank} is given by the pressure difference between the end and the beginning of the operation point, and ΔQ_{stack} can be computed by numerically integrating the measured stack current during the steady operation point. Then a linear regression can be fitted to minimize the squared errors and find the Faradaic efficiency, which should be very close to 100%. To use equation 31 for fitting, we should have an estimate of the tank temperature, T_{tank} . As there's no measurement on this point, we assumed it to be constant at 20 °C at first.

Using linear regression, with $T_{tank} = 20$ [°C], we obtained $\eta_F = 103.6\%$ (95% CI = [99.3 , 107.8]). There could be many reasons why this calculated value is above 100%:

- The noise in the pressure data may not be completely smoothed which causes an instability in pressure differences.
- The stack current may be undermeasured during the erroneous measurement points, so the charge passing through the stack is underestimated, which results in less charge and more pressure, i.e. higher efficiency.
- As the tank pressure sensor is located directly at the output of the stack and not in the tanks, the temperature of this area may be affected by the stack, resulting in a higher pressure reading for less charge, i.e. higher efficiency.
- The real tank temperature can be higher.

We conclude that more experiments should be made in order to have a more accurate prediction on the evolution of the tank pressure. At the time of writing this report, there was no possibility of further experiments because of technical issues, so another regression is performed at $T_{tank} = 30$ [°C], and $\eta_F = 100.2\%$ (95% CI = [96 , 104]) is obtained. It's theoretically impossible to have a Faradaic efficiency more than 100%, however, we conclude that this result shows more or less that the assumptions can be considered valid, and η_F can be taken as 100% for the sake of simplicity.

2.3.2 Tank filling simulations

The tank pressure change in time can be simulated using the model in figure 24. According to the model, it should be possible to predict the pressure change in time by knowing the stack current. As two different tank pressures were considered previously, the simulations were made on two different tank temperatures.

The simulations that were done in Simulink are shown in figures 26 and 27. Given a stack current dispatch plan, we clearly see that the both models are almost completely successful when predicting the tank pressure 1-hour ahead.

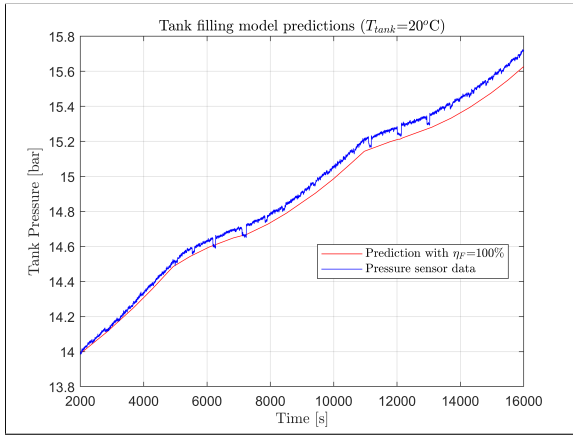


Figure 26: Pressure simulations at 20°C

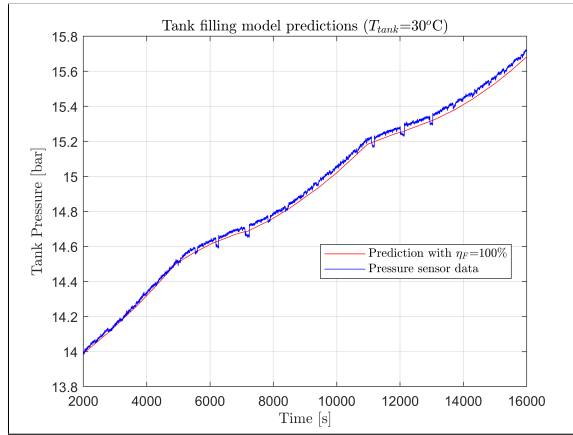


Figure 27: Pressure simulations at 30°C

Considering η_F equal to 100%, and using the stack model in equation 26 and the efficiency curves in figure 23, we can predict the generated hydrogen at a given operating point (power and temperature) as shown in figures 28 and 29.

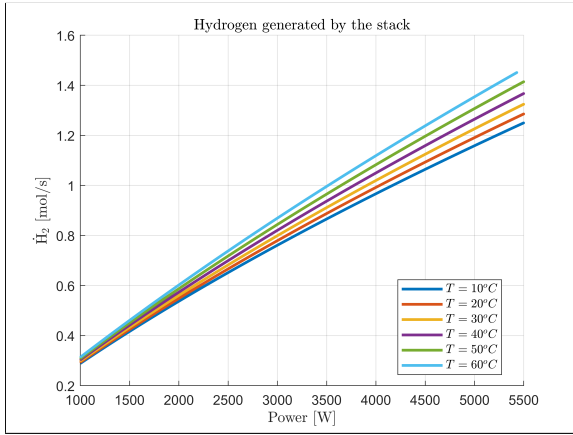


Figure 28: Hydrogen generation model

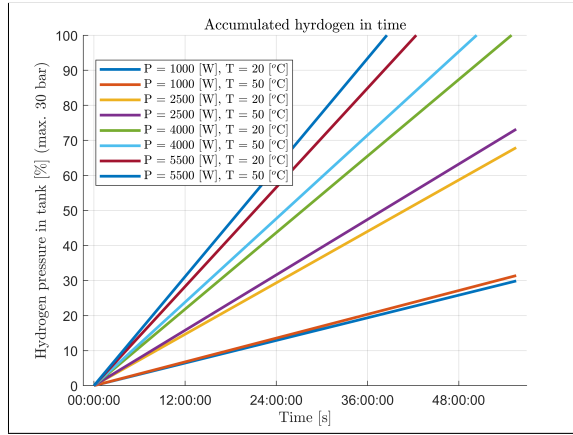


Figure 29: Accumulated fuel in time

2.4 Thermal Model

For the electrical stack model presented in section 2.2, the temperature was an exogenous variable. However, we know that the temperature of the stack is a consequence of the generated heat, and it can be manipulated using the cooling system. For this reason, we will use a thermal model which will allow us to predict the stack temperature in terms of the operating point (power) and other parameters that we can choose. This would simplify the control from the grid's point of view, as we can only use the power as a control variable. The model's diagram is presented in figure 30. T_{cool} represents the cooling setpoint of the cooling system that we can adjust manually, P_{in} and P_{out} are the instantaneous input and output powers of the stack. Having the electrical model in section 2.2, for a given T_{stack} , it's straightforward to calculate the generated heat (losses). And having the losses, it should be again straightforward with the thermal model to calculate the T_{stack} to be fed back in the stack model as in figure 2.

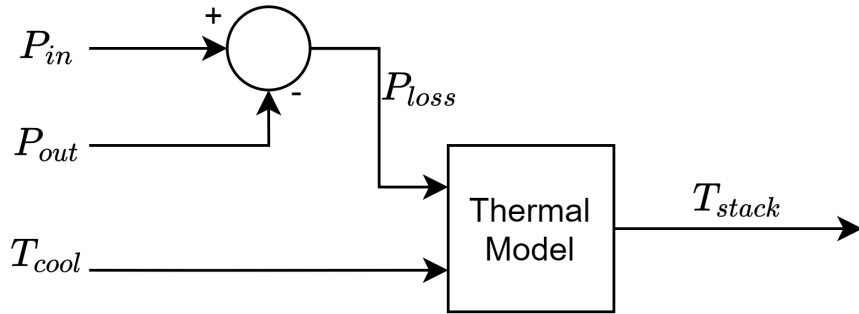


Figure 30: Thermal model diagram

2.4.1 Thermal circuit

[4], [8] and many in [2] use the same thermal model for an electrolyzer stack. We will represent this model with an electrical circuit analogy as shown in figure 31. \dot{Q}_{loss} and \dot{Q}_{cool} are respectively the heat flow generated by the power losses and extracted by the cooling system in units $[J/s] = [W]$, C_{th} is the lumped thermal capacitance of stack in $[J/\text{°C}]$, R_{th} is the thermal resistance in $[K/W]$ representing the heat dissipated to the ambient air and T_{amb} is the temperature source representing the ambient air temperature in $[K]$.

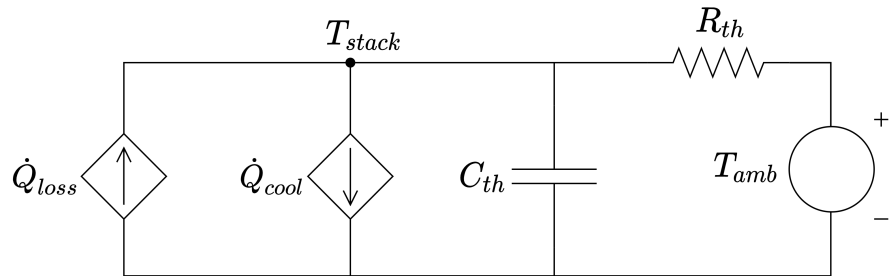


Figure 31: Thermal circuit

The thermal circuit gives the equation:

$$\dot{Q}_{loss} = \dot{Q}_{cool} + C_{th} \frac{dT_{stack}}{dt} + \frac{T_{stack} - T_{amb}}{R_{th}} \quad (32)$$

This model is represented in Laplace domain as in equation 33, where the heat caused by the losses is equal to the power loss of the stack, and P_{cool} signifies heat flow extracted by the cooling system.

$$T_{stack} = \frac{R_{th} (P_{loss} - P_{cool}) + T_{amb}}{1 + sR_{th}C_{th}} \quad (33)$$

This representation then can be used to simulate the stack temperature if the behavior of the cooling system can be determined. Figure 32 shows the implemented model in Simulink.

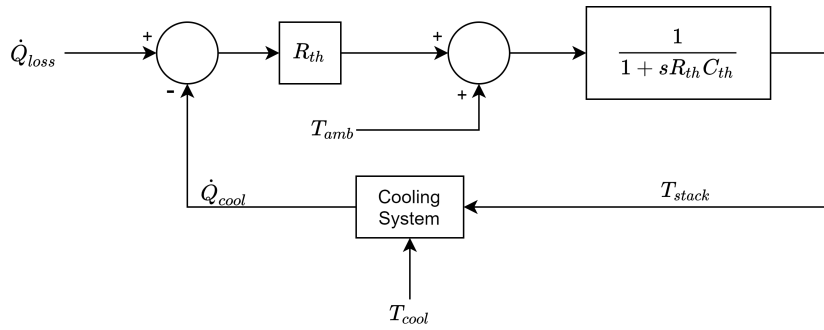


Figure 32: Thermal circuit simulation implementation

2.4.2 Estimation of passive components

As we haven't done any additional experiment for the thermal model due to technical issues, we will use the electrical stack model experiment dataset in figure 18 and extract the meaningful data from it.

We will first need to determine two passive parameters for the thermal model: C_{th} and R_{th} . To determine these values, we use the data extracted from the beginning of the experiment, where the temperature of the stack is rising naturally because of the losses and the cooling system hasn't been activated yet. We see from the logfiles that during the first 1600 seconds of the experiment, the cooling system is off. This can be seen in figure 33 where the power losses are computed using the hydrogen generation model and the electrical model.

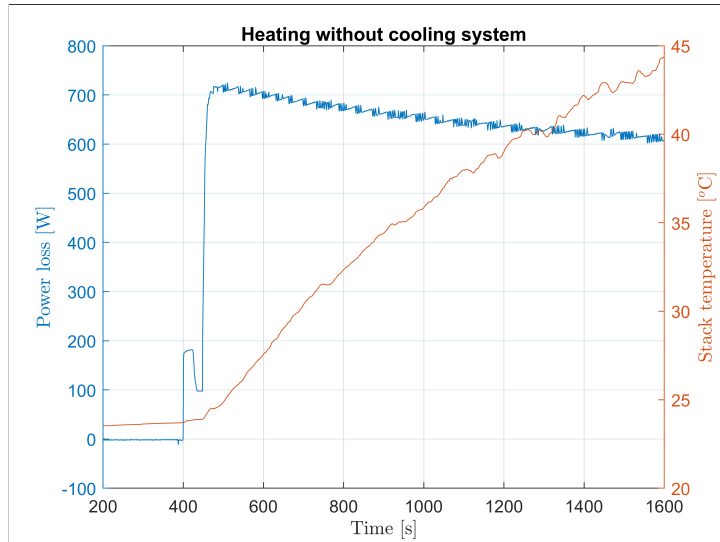


Figure 33: Loss step without cooling system

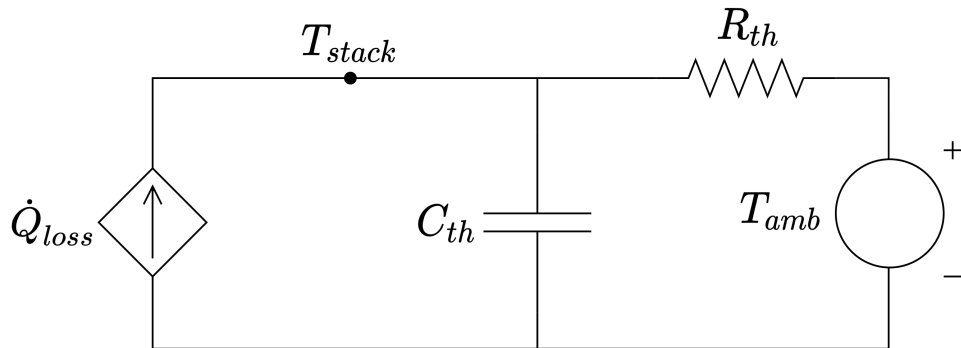


Figure 34: Thermal circuit without cooling system

The thermal circuit without the cooling system can be seen in figure 34. We can empirically try to estimate the two passive elements of the thermal circuit:

- C_{th} can be estimated using the first instants of the step response. Before the step, the stack temperature is constant at ambient temperature. Then, when a step loss is applied, all the additional heat will first flow to the lumped capacitance in order to be able to increase the temperature exactly as in an electrical RC circuit. Thus, the slope of the temperature change at the beginning of the step response is given by (where E_{loss} corresponds to the total energy lost by the stack during a given time) :

$$C_{th} \cdot \frac{dT_{stack}}{dt} = \dot{Q}_{loss} \quad \Rightarrow \quad \Delta C_{th} \approx \frac{\dot{Q}_{loss} \Delta t}{\Delta T_{stack}} = \frac{E_{loss}}{\Delta T_{stack}} \quad (34)$$

We use the first 200 seconds of the step response, we numerically integrate the power losses to find the lost energy and simply use the temperature difference during 200 seconds to find $C_{th} = 29.3 \text{ kJ/K}$.

- To calculate R_{th} , we can use the time constant ($\tau = R_{th}C_{th}$) of the system. If we had an opportunity to do many thermal tests, we could fit a τ again with OLS regression as we did in section 2.1.2. As we're not able to do that, we will use the simulation to predict the stack temperature during natural heating, and experimentally choose the best R_{th} that fits the predicted curve on the measurement. We see in literature that the estimated time constants are around 3000 s. For example, [4] finds a time constant of 3435 s for its stack. Considering that value, we took an initial guess for R_{th} to start, and we picked a value of 0.1 [K/W]. We see that this already gives a good approximation, as seen in figure 35. The time constant is also validated in figure 36, where the cooling system had turned itself off for 8 minutes, because cooling temperature setting was raised from 30 °C to 50 °C.

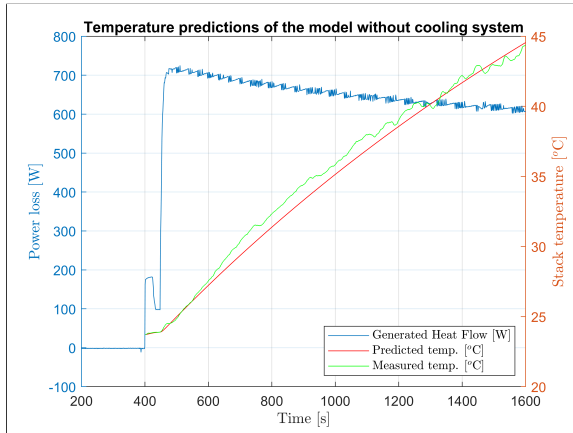


Figure 35: Step loss temperature simulation

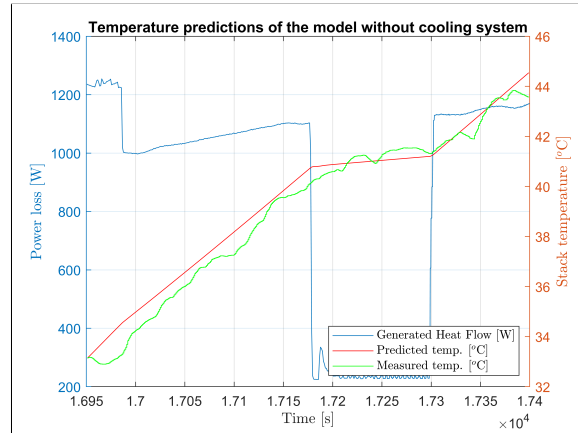


Figure 36: Natural heating simulation

2.4.3 Cooling system model

The cooling system is controlled using a given reference temperature parameter as shown in figure 32. We observed the effect of a step change in the cooling temperature on the stack temperature in figure 37.

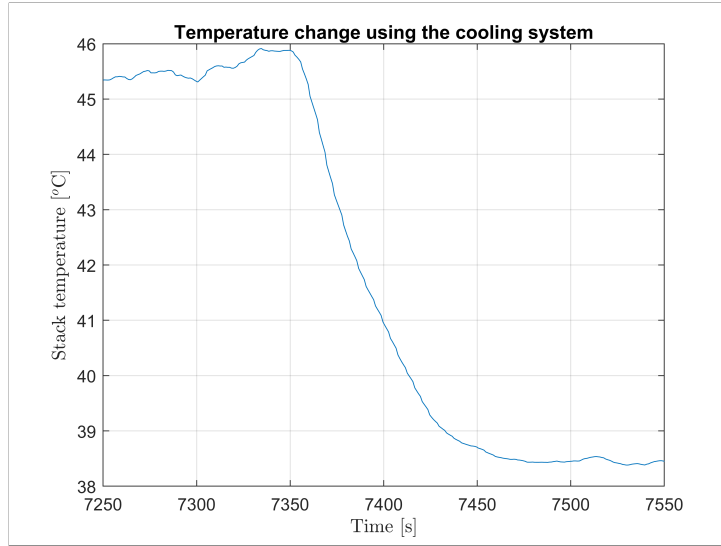


Figure 37: Cooling step response

Referring to figure 37, with a rough approximation, we can say that a step of \dot{Q}_{cool} is applied as the cooling temperature changed instantly. The time constant is observed to be around 50 seconds. By doing the same as in equation 34, seen from the figure that the cooling system is able to decrease the temperature by 5 °C in 50 seconds, we get:

$$\dot{Q}_{cool} = \frac{\Delta T_{stack} \cdot C_{th}}{\Delta t} \approx 2.8 \text{ kW}$$

This shows that the cooling system is able to take away roughly 2.8 kJ of heat each second when running at full capacity. To demonstrate this, a simulation with an on-off controlled cooling system with $\dot{Q}_{cool} = 2.8 \text{ kW}$ is given in figure 38. However, one should note that the control system behind the cooling system is much more complex in reality. An on-off controller is just a brutal approximation to verify that the cooling controller is in fact much more aggressive

than the natural heating of the stack. If that's true, we can consider stable operation on fixed temperatures. This assumption is discussed in the next subsection.

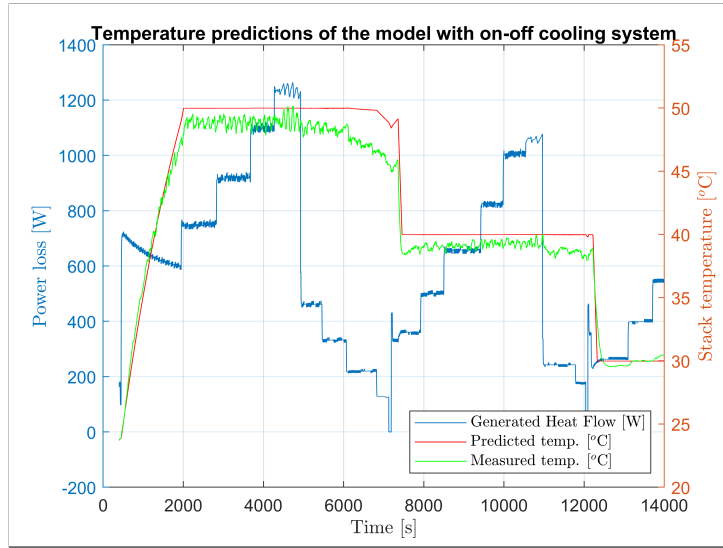


Figure 38: Simulation with on-off cooling system

2.4.4 Temperature assumption and model simplification

It's shown in the previous subsection that the cooling system is much more aggressive than the passive heating elements of the system, and it easily overcomes the heat generated by the losses. Thus, it is able to stabilize the temperature around some working point by extracting the excess heat.

We know from section 2.2 that we get a better efficiency at higher temperatures. However, the provider suggests working at temperatures less than 50 °C, to preserve the lifetime of the stack. Thus, the input parameter T_{cool} can be fixed to any value under 50 °C, and the stack temperature can be assumed constant for the sake of simplicity. To guarantee better efficiency at each power level, 50 °C is the value to choose.

3 Conclusion

After briefly analyzing each submodel, we concluded that the system in fact can very much be simplified and we obtained promising models.

- For the power tracking model, we estimated a time constant which showed good reproducibility on different reference power steps. We found the time constant using two methods and visualized the prediction results. However, the step-down behavior when the step is more than 2 kW is left unexplained because of the impossibility of realizing new experiments, and due to connection problems with stack provider at the time of writing this report. To describe the negative-step, the same approach could be used if more experiments could be done. This model can still be used in a control loop if one can make sure that the negative step on the power references won't reach 2 kW.
- For the stack model, we were able to describe the voltage of the stack in terms of a given stack current and stack temperature by an empirical and massively simplified approach.

This model allowed us to reduce the degrees of freedom. By using this model and the tank model together, we were able to describe the filling time of the tank, generate efficiency curves for different power levels and find other important control parameters. In section 2.4.4, we saw that we can work at a nearly fixed temperature $T_{stack} \approx 50^{\circ}\text{C}$ and further simplify our model.

- The tank model and the hydrogen production model allowed us to calculate and verify the fuel accumulated in the tank. We saw that the Faradaic efficiency is very high, and we even calculated unrealistically high values using the measurements. By considering the Faradaic efficiency at 100%, we were able to predict the 1-hour ahead tank pressure almost perfectly for a given current dispatch plan.
- Using the thermal model, we were able to explain how fast the stack heats up and cools down. We simulated the stack temperature without the cooling system and obtained promising results. We showed that the cooling system is much more powerful than the natural heating of the stack. Using this result, we simulated an overpowered on-off controller along with the thermal model, and showed that the cooling system can stabilize the stack temperature very successfully, like an overpowered on-off controller, around some defined temperature levels.

Finally, the simplified system is given in figure 39.

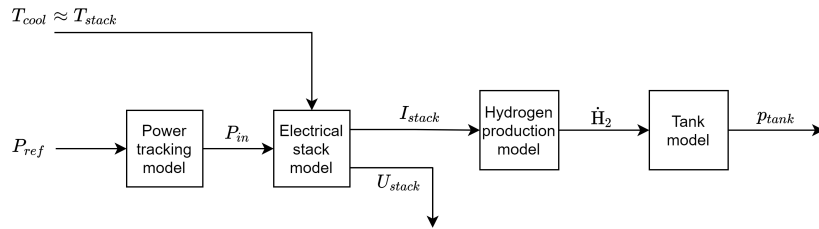


Figure 39: Simplified system

Appendix: MATLAB Files

The plots, simulations and models in this report were prepared in MATLAB and Simulink, and should be found attached. Please see the corresponding .mlx file for the plots and analysis concerning the models. Below, we also include some short descriptions of the files.

```

files
├── Electrical_stack_model
│   ├── electrical_model mlx      Contains the stack model & efficiency curves.
│   └── model_fit.m      Helper function.
├── Power_reference_tracking
│   ├── tracking_model mlx      Contains the power reference tracking model.
│   ├── OLS_beta.m      Helper function.
│   ├── firstorder_step_resp_unitary.m      Helper function.
│   └── first_order_tau_estimator.m      Helper function.
├── Tank_and_production
│   ├── production_tank_model mlx      Contains the production and tank models.
│   ├── tankfill_fit.m      Helper function.
│   └── filling_model.slx      Used to simulate the tank pressure.
└── Thermal_model
    ├── thermal_analysis mlx      Contains the thermal model
    └── Thermal_model.slx      Used to simulate the stack temperature

```

References

- [1] F. Sossan, H. Bindner, H. Madsen, D. Torregrossa, L. R. Chamorro, and M. Paolone, “A model predictive control strategy for the space heating of a smart building including cogeneration of a fuel cell-electrolyzer system,” *International Journal of Electrical Power & Energy Systems*, vol. 62, pp. 879–889, 2014, ISSN: 0142-0615. DOI: <https://doi.org/10.1016/j.ijepes.2014.05.040>. [Online]. Available: <https://www.sciencedirect.com/science/article/pii/S0142061514003111>.
- [2] D. Falcão and A. Pinto, “A review on pem electrolyzer modelling: Guidelines for beginners,” *Journal of Cleaner Production*, vol. 261, p. 121184, 2020, ISSN: 0959-6526. DOI: <https://doi.org/10.1016/j.jclepro.2020.121184>. [Online]. Available: <https://www.sciencedirect.com/science/article/pii/S0959652620312312>.
- [3] R. Gupta, F. Sossan, and M. Paolone, “Grid-aware distributed model predictive control of heterogeneous resources in a distribution network: Theory and experimental validation,” *IEEE Transactions on Energy Conversion*, Aug. 2020. DOI: 10.1109/TEC.2020.3015271.
- [4] R. García-Valverde, N. Espinosa, and A. Urbina, “Simple pem water electrolyser model and experimental validation,” *International Journal of Hydrogen Energy*, vol. 37, no. 2, pp. 1927–1938, 2012, 10th International Conference on Clean Energy 2010, ISSN: 0360-3199. DOI: <https://doi.org/10.1016/j.ijhydene.2011.09.027>. [Online]. Available: <https://www.sciencedirect.com/science/article/pii/S0360319911021380>.
- [5] F. Marangio, M. Santarelli, and M. Calì, “Theoretical model and experimental analysis of a high pressure pem water electrolyser for hydrogen production,” *International Journal of Hydrogen Energy*, vol. 34, no. 3, pp. 1143–1158, 2009, ISSN: 0360-3199. DOI: <https://doi.org/10.1016/j.ijhydene.2008.11.083>. [Online]. Available: <https://www.sciencedirect.com/science/article/pii/S0360319908016571>.

- [6] V. Fourmond and C. Léger, “Chapter 9 - an introduction to electrochemical methods for the functional analysis of metalloproteins,” in *Practical Approaches to Biological Inorganic Chemistry (Second Edition)*, R. R. Crichton and R. O. Louro, Eds., Second Edition, Elsevier, 2020, pp. 325–373, ISBN: 978-0-444-64225-7. DOI: <https://doi.org/10.1016/B978-0-444-64225-7.00009-2>. [Online]. Available: <https://www.sciencedirect.com/science/article/pii/B9780444642257000092>.
- [7] M. Shen, N. Bennett, Y. Ding, and K. Scott, “A concise model for evaluating water electrolysis,” *International Journal of Hydrogen Energy*, vol. 36, no. 22, pp. 14335–14341, 2011, Fuel Cell Technologies: FUCETECH 2009, ISSN: 0360-3199. DOI: <https://doi.org/10.1016/j.ijhydene.2010.12.029>. [Online]. Available: <https://www.sciencedirect.com/science/article/pii/S0360319910023712>.
- [8] R. CHEVALIER, Modelization of a PEM electrolyzer, Master Project at EPFL.
- [9] W. Wang, X. Wei, D. Choi, X. Lu, G. Yang, and C. Sun, “Chapter 1 - electrochemical cells for medium- and large-scale energy storage: Fundamentals,” in *Advances in Batteries for Medium and Large-Scale Energy Storage*, ser. Woodhead Publishing Series in Energy, C. Menictas, M. Skyllas-Kazacos, and T. M. Lim, Eds., Woodhead Publishing, 2015, pp. 3–28, ISBN: 978-1-78242-013-2. DOI: <https://doi.org/10.1016/B978-1-78242-013-2.00001-7>. [Online]. Available: <https://www.sciencedirect.com/science/article/pii/B9781782420132000017>.